Surface enhanced Raman spectroscopy (SERS) of bacterial metabolites for bacterial growth monitoring and diagnosis of viral infection

Wei Wang, [†‡] *Seju Kang,* [†‡] *and Peter J. Vikesland* *[†‡]

[†] Department of Civil and Environmental Engineering, Virginia Tech, Blacksburg, Virginia 24061, United States

[‡] Virginia Tech Institute of Critical Technology and Applied Science (ICTAS) Sustainable Nanotechnology Center (VTSuN), Blacksburg, Virginia 24061, United States

*Corresponding Author: Peter J. Vikesland; Email: pvikes@vt.edu.

ABSTRACT: Bacterial metabolites are intermediate products of bacterial metabolism and their production reflects metabolic activity. Herein, we report the use of surface enhanced Raman spectroscopy (SERS) for detection of both volatile and non-volatile metabolites and the application of this approach for bacterial growth quantification and diagnosis of viral infection. The time dependent SERS signal of the volatile metabolite dimethyl disulfide (DMDS) in the headspace above bacteria growing on an agar plate was detected and quantified. In addition, SERS signals arising from the plate reflected nutrient consumption and production of non-volatile metabolites. The measurement of metabolite accumulation can be used for bacterial quantification. In the presence of bacteriophage virus, bacterial metabolism is suppressed, and the relative decrease in SERS intensity reflects the initial virus concentration. Using multivariate analysis, we detect viral infection with a prediction accuracy of 93%. Our SERS based approach for metabolite production monitoring provides new insight towards viral infection diagnosis.

KEYWORDS: Surface enhanced Raman spectroscopy, detection, metabolite, bacteria, virus

SYNOPSIS: Surface enhanced Raman spectroscopy enables monitoring of volatile and non-volatile bacterial metabolites, the quantification of bacterial growth, and diagnosis of viral infection.

Graphical abstract:

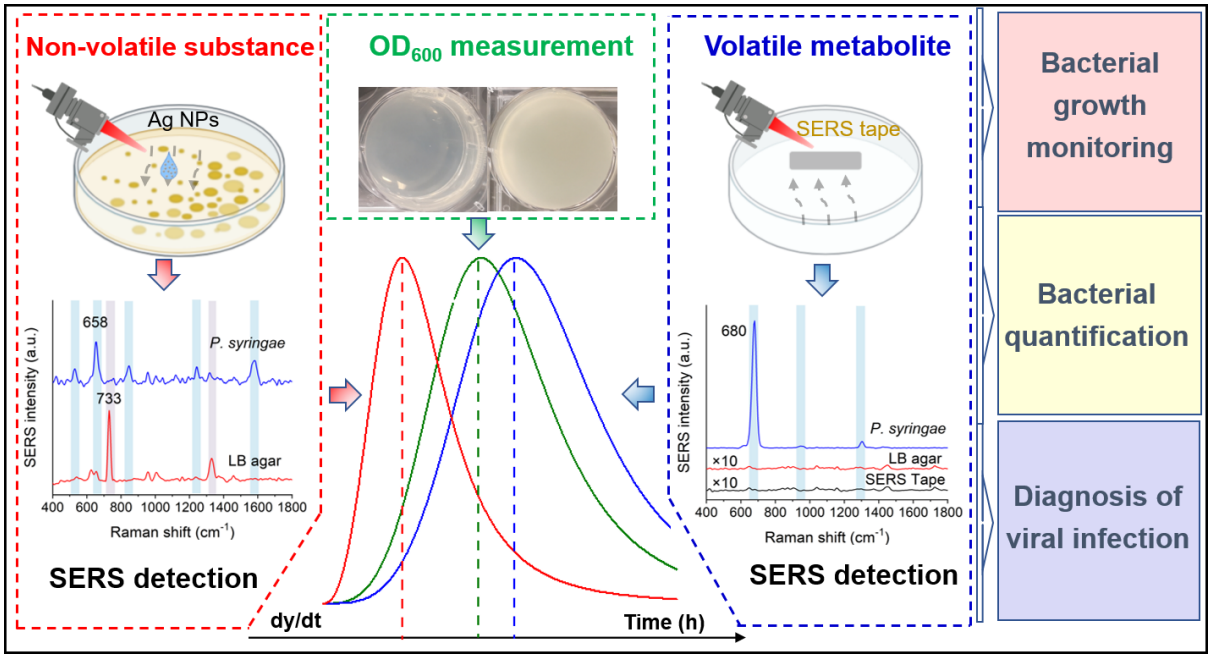
Non-volatile substance
Ag NPs
658
733
P. syringae
LB agar
SERS intensity (a.u.)
400 600 800 1000 1200 1400 1600 1800
Raman shift (cm-1)
SERS detection
OD600 measurement
dy/dt
Time (h)
Volatile metabolite
SERS tape
680
P. syringae
×10
LB agar
×10
SERS Tape
SERS intensity (a.u.)
400 600 800 1000 1200 1400 1600 1800
Raman shift (cm-1)
SERS detection
Bacterial growth monitoring
Bacterial quantification
Diagnosis of viral infection

35

36 **INTRODUCTION**

37 Bacterial metabolites, the intermediate products of bacterial metabolism, reflect the growth,
38 development, and interactions of bacteria with their environment.[1-3] Bacterial metabolites
39 include both soluble and volatile compounds and some of them are highly specific to a given
40 bacterial species.[4] The types and concentrations of metabolites produced are often affected by
41 the environment surrounding a bacterial cell.[5,6] For example, quorum sensing bacteria produce
42 and release autoinducer signaling molecules that regulate gene expression in response to
43 population density fluctuations;[7] and many bacteria produce bacteriocins (e.g., colicin[8]) to
44 control competing species densities when hunting for nutrients or space.[4] Metabolite sensing
45 is considered an important requirement for controlling microbial growth and improving disease
46 diagnosis.[9,10]

47 Many bacterial metabolites are low molecular weight compounds and accordingly gas
48 chromatography-mass spectrometry (GC-MS), liquid chromatography-MS (LC-MS) and their
49 derivatives are often used for metabolite detection.[11-14] However, despite their accurate and
50 robust utility, these conventional methods are complex, time-consuming, and expensive and
51 are inappropriate for rapid point of care or real time measurements. Recently, colorimetric and
52 electrochemical methods have been developed to enable precise *in-situ* metabolite detection.[15-
53 19] These newer detection methods are often designed for targeted sensing that may hinder their
54 capacity to detect unknown chemical species within complex metabolite mixtures. Accordingly,
55 new strategies for the detection of bacterial metabolites are attracting significant attention.

56 Surface-enhanced Raman spectroscopy (SERS) is an ideal approach for biological sensing
57 due to its high sensitivity, real time response, and capacity for molecular fingerprinting.[20,21]
58 The Raman scattering of an analyte can be significantly enhanced when it is located within the
59 strong electromagnetic field generated by the localized surface plasmon resonance (LSPR) of
60 plasmonic nanoparticles.[22] SERS can be used to capture spectral fingerprints of biomolecules

61 without the use of labels and can achieve ultrahigh sensitivity.[23] Recently, a number of
62 researchers have used SERS for bacterial metabolite detection.[24-27] SERS substrates can either
63 be placed near bacteria to evaluate intracellular or local extracellular metabolites[27] or can be
64 placed in the headspace to detect gaseous metabolites.[28-30] *In-situ* SERS of signaling
65 metabolites has been obtained using purposely designed substrates to understand both
66 intraspecies communication[27,31] as well as interspecies interactions within complex microbial
67 communities.[32,33] Besides end-point detection, time dependent SERS signals can provide real
68 time information about metabolite production, which can then be used to define metabolic
69 activity.[30,34] These studies have collectively shown that SERS is a promising means for
70 metabolite sensing. However, up until now, research has focused more on metabolite detection
71 and only a few papers monitoring of bacterial growth or metabolite quantification.[27]

72 Since metabolic activities can be affected by environmental conditions, SERS metabolite
73 signals can be used to examine the effects of external stimuli such as antibiotic treatment.[35,36]
74 Bacteriophage viruses are well-recognized elements to bacterial mortality.[37] Following
75 bacteriophage infection, the host bacterial metabolism is altered in favor of viral replication
76 and in the case of lytic viruses may ultimately result in bacterial cell rupture. For this reason,
77 bacteriophages have been suggested as an alternative means of bacterial inactivation in lieu of
78 antibiotics.[38,39]

79 In the present study, we report that bacterial metabolite SERS signals can be used for
80 bacterial growth monitoring and the diagnosis of viral infection. Instead of focusing on one or
81 two representative metabolites as done previously, we simultaneously detected both volatile
82 and non-volatile metabolites. To do so, we prepared a low-cost plasmonic substrate that could
83 be inverted inside the cover of a Petri dish to passively capture volatile metabolites formed
84 during bacterial cultivation (**Scheme 1**). To detect non-volatile substances, colloidal
85 nanoparticles were directly pipetted onto the culture plate. The collected SERS signals of the

86 metabolites were used to monitor bacterial growth and for bacterial quantification. To diagnose
87 viral infection, variable virus titers were added to the bacterial culture, the resulting SERS
88 signals were recorded, and multivariate analysis was used for classification. The lytic
89 bacteriophage Phi6, a surrogate for enveloped viruses, such as SARS-CoV-2 and influenza
90 virus,[40-42] and its host bacteria *Pseudomonas syringae* (*P. syringae*) were used in these proof-
91 of-concept studies. The approach described in this work, based on SERS monitoring of
92 bacterial host metabolites, provides new insight into viral infection diagnosis.

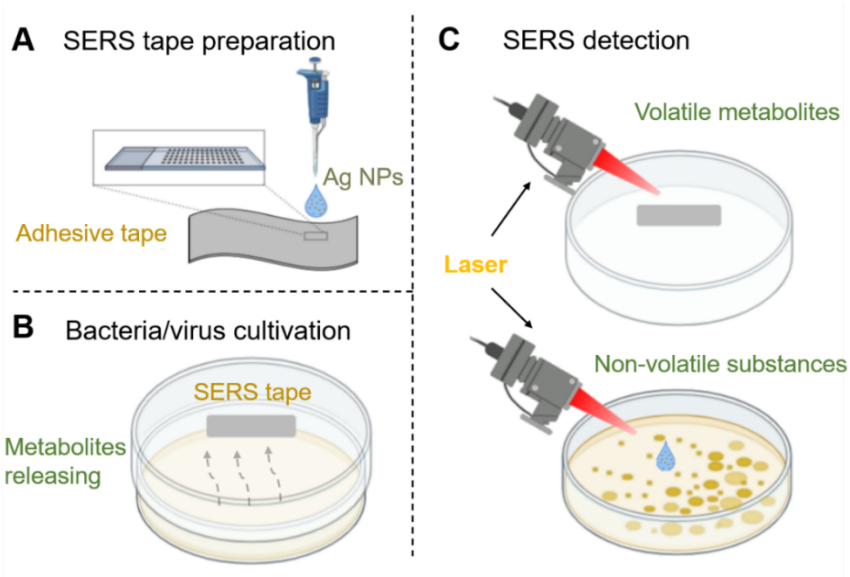

93

94 **Scheme 1.** Schematic illustration of (A) SERS substrate preparation; (B) bacterial cultivation
95 with/without virus; (C) SERS detection for both volatile and non-volatile metabolites.
96

97 **EXPERIMENTAL SECTION**

98 **Materials.** Silver nitrate ($AgNO_3$, 99%), hydroxylamine hydrochloride ($NH_2OH{\cdot}HCl$, 99%),
99 sodium hydroxide (NaOH, ≥ 98.0%), dimethyl disulfide (DMDS, ≥ 99%), and 4-
100 mercaptobenzoic acid (4-MBA, 99%) were purchased from Millipore Sigma. Luria-Bertani
101 (LB) broth (Miller, powder) and agar (Difco, granulated) were obtained from Fisher Scientific.
102 The adhesive tape (Scotch double sided adhesive tape) was purchased from the local market.
103 Bacterial stains *Pseudomonas syringae* pv phaseolicola (*P. syringae*), *Escherichia coli* K 12
104 (*E. coli*), and bacteriophages Phi6, MS2 were obtained from Dr. Linsey Marr's group.[40,43]

105 Deionized water from a Milli-Q-plus system was used throughout this work.

106 **Synthesis of colloidal silver nanoparticles (AgNPs) and SERS substrate.** The colloidal
107 suspension of AgNPs was synthesized via a facile and fast preparation method at room
108 temperature.[44] Briefly, 9 mL of 2 mmol/L freshly prepared $NH_2OH \cdot HCl$ solution (containing
109 3 mmol NaOH) was mixed with 1 mL of 10 mmol/L $AgNO_3$ in a centrifuge tube. The mixture
110 was then vortexed for 1 min to achieve complete mixing. During the process, the solution was
111 turned to yellow/greenish. The prepared colloidal AgNPs were stored in the dark at 4 °C for
112 future use.

113 The low-cost SERS tape substrate was fabricated by depositing AgNPs on adhesive tape
114 as reported in the literature.[45] Generally, 50 μL of the as-prepared AgNPs were uniformly
115 pipetted on the surface of the adhesive tape. After being dried naturally at room temperature,
116 AgNPs were readily immobilized on the tape without other modifications and the aggregation
117 of the nanoparticles generated abundant SERS hot spots, where the highest SERS enhancement
118 occurs.[46]

119 **Bacterial cultivation and viral propagation.** Before cultivation, LB medium was prepared
120 by dissolving LB broth (containing 10 g of tryptone, 5 g of yeast extract, and 10 g of NaCl) in
121 1 L water. LB agar plates were made by adding 1.5% agar to the prepared LB medium,
122 autoclaved, and then poured into glass Petri dishes before cooling down. Bacterial strain *P.*
123 *syringae* was steaked onto the LB agar plates and incubated at 25 °C for 48 h. A single colony
124 was transferred to 15 mL of autoclaved LB medium and incubated at 25 °C with agitation (200
125 rpm) for 24 h. The obtained *P. syringae* suspensions were diluted in series and inoculated into
126 LB agar plates and the concentration was obtained by counting colony forming units (CFU)
127 after cultivating for another 48 h.

128 To propagate Phi6, LB soft agar (LB medium with 0.75% agar) was prepared and
129 autoclaved. An aliquot of 4 mL of LB soft agar was pipetted to each culture tube and kept in a

130 50 °C water bath. Then, 200 μL of the *P. syringae* suspensions and 50 μL of Phi6 stock were
131 added to the culture tubes. The mixture was poured on top of a LB agar plate and cultured at
132 25 °C for 24 h. Phi6 was harvested by scraping soft agar from the plate into a 50 mL centrifuge
133 tube with 5 mL of LB medium. The tube was vortexed and centrifuged for 10 min at 1753×g.
134 Bacterial cells and debris were removed from the Phi6 suspension by filtering through a 0.22
135 μm cellulose acetate membrane. Plaque forming units (PFU) were counted by repeating the
136 abovementioned procedure with different Phi6 dilutions. *E. coli* and MS2 were cultured with
137 the same procedures but at 37 °C.

138 **SERS monitoring of bacterial metabolites.** The SERS tape was inversely attached inside the
139 cover of a *P. syringae* containing glass Petri dish. The plate was sealed by parafilm and the
140 released volatile metabolites were captured by the substrate. After 24 h incubation, the SERS
141 signals were recorded. The SERS signals of non-volatile substances were obtained by directly
142 pipetting 5 μL of prepared AgNPs onto the culture plate. To evaluate metabolite release and
143 cell growth, the bacterial optical density (OD_{600}) was measured at 10 min intervals and the
144 SERS signals were recorded at 3 h intervals over a 24 h period. To diagnose viral infection, 50
145 μL of Phi6 (10^7 PFU/mL or diluted) was pre-added to 200 μL of 10^9 CFU/mL *P. syringae*
146 suspension. SERS data were then collected after 24 h incubation. All the other procedures were
147 as stated previously.

148 **Instrumentation.** A field-emission Quanta 600 FEG environmental scanning electron
149 microscope (SEM) was used to observe the morphologies of AgNPs and SERS Tape.
150 Ultraviolet-visible (UV-Vis) spectrophotometer (Cary 5000, Agilent) and dynamic light
151 scattering instruments (DLS, Zetasizer Nano ZS) were used to obtain the UV-Vis spectrum and
152 hydrodynamic diameter of AgNPs, respectively. A microplate reader (Multi-mode, Synergy™
153 HTX) was adapted to measure OD_{600}. WITec alpha500R Raman spectrometer (WITec GmbH,
154 Ulm, Germany, spectral resolution = ~3.5 cm^{-1}) with a 785 nm laser and a 10× confocal

155 microscope objective was used to obtain the SERS spectra of all the samples. The silicon peak
156 at 520 cm^{-1} was used for instrumental calibration before measurement. The signal was collected
157 using a Peltier cooled charge coupled device (CCD) with 300 Groves per mm grating set. For
158 each sample, 400 spectra (20×20; X×Y) were acquired across a 100×100 μm^2 area with an
159 integration time of 0.1 s for each point.

160 **SERS data analysis.** The instrument embedded software (Project Five) was used for spectral
161 cosmic ray removal, Savitzky-Golay smoothing, baseline subtraction, and peak identification.
162 Subsequently, the SERS data was analyzed using MATLAB® 2019b (The MathWorks, USA)
163 to calculate the absolute intensities of the peak of interests and the ratio of different peaks.
164 Multivariate data analysis was also performed in MATLAB. Principal component analysis
165 (PCA) was employed to identify the spectral features within 400 to 1800 cm^{-1} during bacterial
166 growth. To diagnose viral infection, 18 spectral features were selected by the software from a
167 total of 3600 spectra (2000 spectra for infected *P. syringae* and 1600 spectra for normal *P.*
168 *syringae*). Support vector machine (SVM) classification with quadratic kernel function was
169 performed to help differentiate multivariate SERS data.

170

171 **RESULTS AND DISCUSSION**

172 **Characterization of AgNPs and SERS tape.** AgNPs were synthesized by room temperature
173 hydroxylamine hydrochloride reduction.[44,47] As prepared, spherical AgNPs exhibited high
174 uniformity and a TEM determined average size of 44.8 ± 8.6 nm (**Figure S1**). When dispensed
175 in water, the AgNPs exhibited the expected LSPR band at ≈410 nm[47] and a DLS determined
176 average hydrodynamic diameter (Z_{ave}) of 79.6 ± 22.8 nm. The SERS tape substrate was
177 fabricated by uniformly depositing AgNP suspension (≈2×10^9 NPs/mL) on the sticky layer of
178 commercially available double-sided adhesive tape. Once dried, the AgNPs aggregated and
179 became embedded on the tape surface due to the swelling and deswelling action of the

180 adhesive.[45] After decoration, the morphology of the tape surface changed from smooth and flat
181 to rough (**Figure S2**).

182 In proof-of-concept experiments, the SERS performance of both the AgNPs and the SERS
183 tape was evaluated. The responsive, pH sensitive SERS molecule 4-MBA was chosen to verify
184 our methods. AgNPs were mixed with 4-MBA and placed on the surface of aluminum foil as
185 droplets, while the SERS tape dried naturally after 4-MBA solution was added. As shown in
186 **Figure 1**, both AgNPs and SERS tape showed high SERS performance towards 4-MBA with
187 SERS enhancement factors of 5×10^7 and 3×10^7, respectively. The SERS results exhibited large
188 spatial variations due to the heterogeneous distribution of hot spots, especially for SERS tape
189 (coefficient of variation (CV) = 46.0%, **Figure 1E**). The AgNPs self-aggregated on the tape
190 and the aggregation process was uncontrolled, thus resulting in the random spatial distribution
191 of SERS hot spots. We have recently reported on the use of surface enhanced elastic scattering
192 as a localized intrinsic internal standard to address hot spot variability and improve SERS
193 reproducibility.[48-50] Succinctly, a pseudo peak at ~77 cm^{-1} (I_{77}), which is the surface enhanced
194 elastic scattering signal, is enhanced within the hot spots. Accordingly, I_{77} can be used as an
195 internal standard for hot spot normalization. Following hot spot normalization, the CV of
196 SERS tape declined to 14.1% (**Figure 1F**), a value comparable to many substrates.[45,51,52]
197 Similarly, the CV of AgNPs alone decreased from 15.2 to 5.9% (**Figures 1B and 1C**). High
198 SERS enhancement, reproducibility, and deployability suggest the promise of SERS tape.

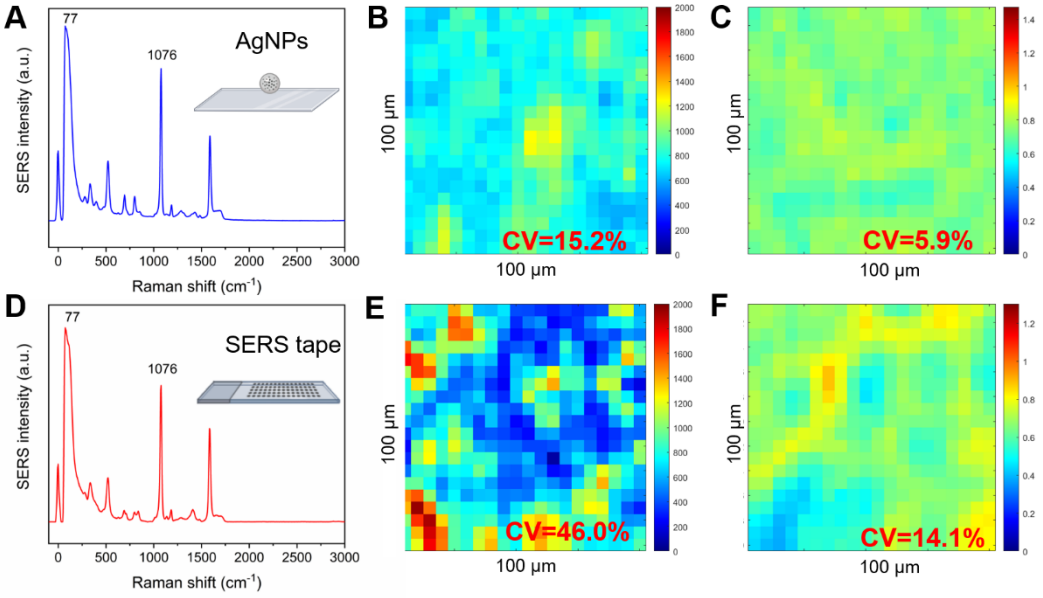

Figure 1. SERS spectra and maps of 4-MBA on AgNPs (A-C) and SERS tape (D-F). (A) and (D) average spectra of 4-MBA; (B) and (E) maps of peak intensity of 1076 cm^{-1} (I_{1076}, CCD cts); (C) and (F) maps of hot spot normalized peak intensity (I_{1076}/I_{77}). 400 spectra (20×20, X×Y) were acquired across a 100×100 μm^2 area.

SERS spectra of bacterial metabolites. We detected both volatile and non-volatile metabolites. To do so, SERS tape was inversely attached inside the cover of a Petri dish used for *P. syringae* cultivation. Volatile metabolites that partitioned to the headspace of the Petri dish interacted with the SERS tape during *P. syringae* growth. After a 24 h exposure period, the spectra of the SERS tape were recorded. In parallel, AgNPs were directly dropped onto the culture plate and the signals produced by non-volatile substances were detected. As shown in **Figure 2A**, compared to the fresh SERS tape and SERS tape in the control sample (LB agar plate without bacteria), a very strong peak appeared at ~680 cm^{-1} in the headspace above *P. syringae*. This peak reflects the ν(C-S) vibration of methyl sulfide.[29] Previous studies have shown that many bacteria fermentatively produce volatile sulfide compounds, such as dimethyl disulfide (DMDS).[53,54] Methyl sulfide is the expected dissociation product of DMDS on Ag and Au surfaces.[30] Less intense peaks at 950, 1305, and 2917 cm^{-1} reflect the $\nu_s(CH_3)$ vibration, CH_3/CH_2 twist, and $\nu(CH)_{syn}$ vibration, respectively.[30,55] These peaks have been reported

218 previously for volatile bacterial metabolites and reflect alkene, alcohol, ketone, or aromatic
219 compounds in the metabolite mixture (**Table S1**).[28-30,56]

220 The SERS signals of the non-volatile substances detected within the LB agar plates are
221 complex due to their biological origin within bacterial cells that precludes simple
222 identification.[20] In addition, there are several components (protein hydrolysates and nucleobase
223 containing substances) in LB culture medium that contribute to the SERS spectra.[57,58] As
224 shown in **Figure 2B**, LB medium exhibits peaks at 626 cm^{-1} (C-C twisting mode in
225 phenylalanine), 733 cm^{-1} (adenine or phosphatidylserine), 957 cm^{-1} (phosphate or C=C
226 deformation), 1006 cm^{-1} (phenylalanine), 1328 cm^{-1} (CH_2/CH_3 wagging mode present in
227 collagen or purine bases) and 1450 cm^{-1} (CH_2/CH_3 deformation of proteins and lipids).[55,58]
228 Following 24 h cultivation of *P. syringae* the majority of the original LB peaks disappeared,
229 while other peaks appeared or increased in intensity (e.g., 658 cm^{-1} (guanine), 842 cm^{-1}
230 (polysaccharides), and 1582 cm^{-1} (phenylalanine, hydroxyproline, tyrosine, etc.)).[55,59] These
231 new peaks reflect production of metabolites or changes within the bacteria themselves. To
232 explore the origin of these peaks, we selected an area in a LB agar plate where only a fraction
233 of the selected scan area contained bacterial colonies (**Figure S3A**). The SERS signals across
234 the full scan area did not significantly differ (**Figure S3B**), thus suggesting that the peaks did
235 not arise from the bacterial cells. Previous Raman/SERS studies have shown that metabolite
236 signals often dwarf those of bacterial cells.[58] We also cultivated *P. syringae* in LB broth for 24
237 h, centrifuged the sample to collect the supernatant, and resuspended the *P. syringae* pellet in
238 PBS (**Figure S3C**). After resuspension in PBS there were no obvious peaks in the spectrum
239 (**Figure S3D**). Instead, the SERS spectrum of the supernatant had very similar peaks to the
240 original sample. This evidence collectively suggests that the new SERS peaks measured within
241 the plate result from extracellular metabolites (**Table S1**) that are produced by bacteria and
242 then diffuse within the agar.

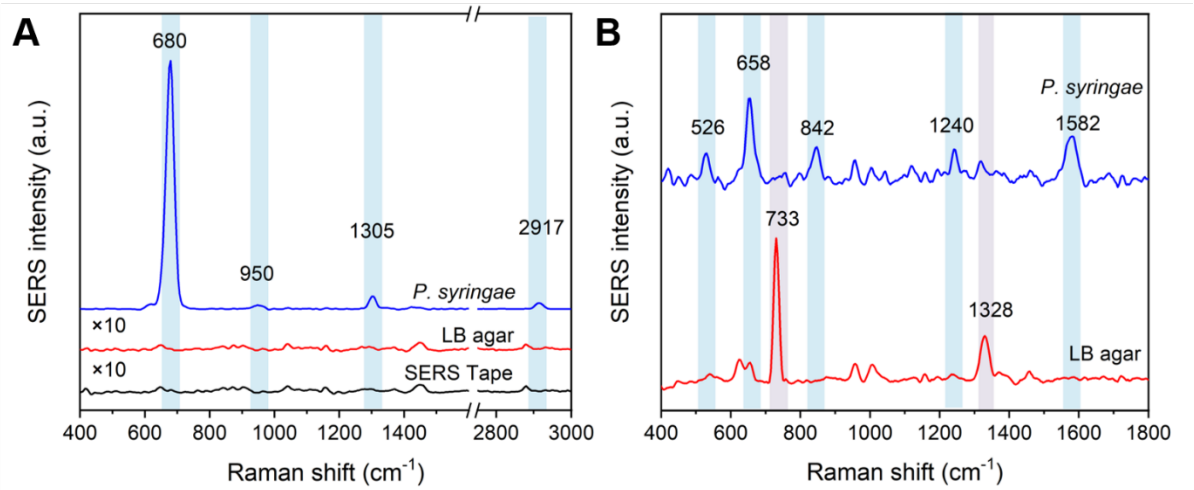

Figure 2. SERS spectra of (A) volatile metabolites in the headspace of *P. syringae* containing culture plate and control plate after 24 h cultivation, and (B) non-volatile substances in LB agar plate before and after 24 h cultivation of *P. syringae*. The light blue bars indicate the characteristic peaks of bacterial metabolites and the light red bars refer to the peaks of LB medium that disappear following cultivation.

Bacterial growth monitoring. To explore the kinetics of metabolite production, SERS spectra were recorded at 3 h intervals and the hot spot normalized peak intensity ($I_{peak\ of\ interest}/I_{77}$) was used for metabolite quantification. For DMDS, as shown in **Figure 3A**, I_{680}/I_{77} increased with time, due to its accumulation in the headspace. After 24 h, the I_{680}/I_{77} ratio was 0.133, corresponding to a headspace concentration of ≈43 μM DMDS (**Figure S4**). For the non-volatile substances, we utilized PCA to identify the peak features that contributed to the greatest differences in the spectra that arise due to bacterial growth (**Figure 3B**). The loading plot of the first principal component (PC1) indicates that spectral features arising from the LB medium (733, 1328, 1006 and 626 cm $^{-1}$) negatively contributed to the loadings (**Figure S5**) and that the normalized intensities of these peaks gradually decreased with time (**Figure S6**) – thus indicating consumption. Relative to the phenylalanine peaks (i.e., 1006 and 626 cm^{-1}), the peaks associated with purines (i.e., 733 and 1328 cm^{-1}) declined considerably within 9 h. The results are consistent with bacterial utilization of exogenous purines as a carbon or nitrogen source.[60,61] Meanwhile, during bacterial growth, the peak initially at ~733 cm^{-1}, which

264 primarily reflects adenine, gradually shifted to ~725 cm^{-1} before it ultimately disappeared. The
265 peak at 725 cm^{-1} reflects hypoxanthine,[62] a typical metabolic intermediate in the formation of
266 nucleic acids, or adenine containing substances[59], such as flavin adenine dinucleotide (FAD)
267 and nicotinamide adenine dinucleotide (NAD). We also examined the normalized intensities
268 of the four peaks that most positively contributed to the PC1 loadings. These peaks reflect
269 production of nucleic acids (658 cm^{-1}), carbohydrates (842 cm^{-1}), and proteins (526, 1582 cm^{-}
270 ^{1}). The most dramatic increase in the four peaks happened between 6-18 h (**Figure S6**),
271 demonstrating production and accumulation of such substances during exponential growth
272 (**Figure 3C**).

273 To better reveal the relationship between the kinetics of metabolite production and
274 bacterial growth, a sigmoidal curve (or 4-parameter logistic model) expressed as
275 $y = m_2 + \frac{m_1 - m_2}{1 + (t / m_3)^{m_4}}$ was used to fit the time dependent data.[63] m_1 and m_2 are the responses
276 (y values) at t=0 and t=∞, respectively, m_3 is the curve inflection point (the point where bacteria
277 have the maximum growth rate), m_4 is the Hill's slope of the curve (slope that defines the
278 steepness of the curve), and t is the time (min). For DMDS, I_{680}/I_{77} was the dependent variable.
279 For non-volatile substances, the ratio of the peaks at 733 and 658 cm^{-1} (I_{733}/I_{658}) was used since
280 the dynamic change in this ratio was larger than the measured change in the I_{658}/I_{77} or I_{733}/I_{77}
281 ratios (**Figure S7**). Accordingly, I_{733}/I_{658} reflects both non-volatile metabolite production and
282 nutrient consumption. To simplify the calculation, we ignored the peak shift at ~733 cm^{-1} and
283 I_{733} represents the intensity of the peak in the range between 725 and 733 cm^{-1}. The fitted
284 parameters are listed in **Table S2**. As shown in **Figures 3D** and **3E**, both I_{680}/I_{77} for DMDS
285 and I_{733}/I_{658} for non-volatile substances were well fitted by the logistic growth model (R^2=0.972
286 and 0.992, respectively) and are consistent with the bacterial growth curve (R^2=0.999). The
287 logistic curves indicate that the detected SERS signals can be directly related to bacterial

growth. By tracking the rate of change in the signal (r=dy/dt; **Figure 3F**), where y is I_{680}/I_{77} or I_{733}/I_{658} for the SERS signals or OD_{600} for bacterial growth, we can see that the rate of change in I_{733}/I_{658} reached a maximum at ~6 h, followed later by the maximum in OD_{600} and then I_{680}/I_{77}. This trend is reflected by the respective m_3 values (**Table S2**). $r(I_{733}/I_{658})$ reflects the synergy between nutrient consumption and the production of non-volatile metabolites. The temporal trends in the rate measurements are consistent with nutrient consumption followed by bacterial growth and metabolite production. DMDS diffusion into the plate headspace may also contribute to the lag in its rate curve.

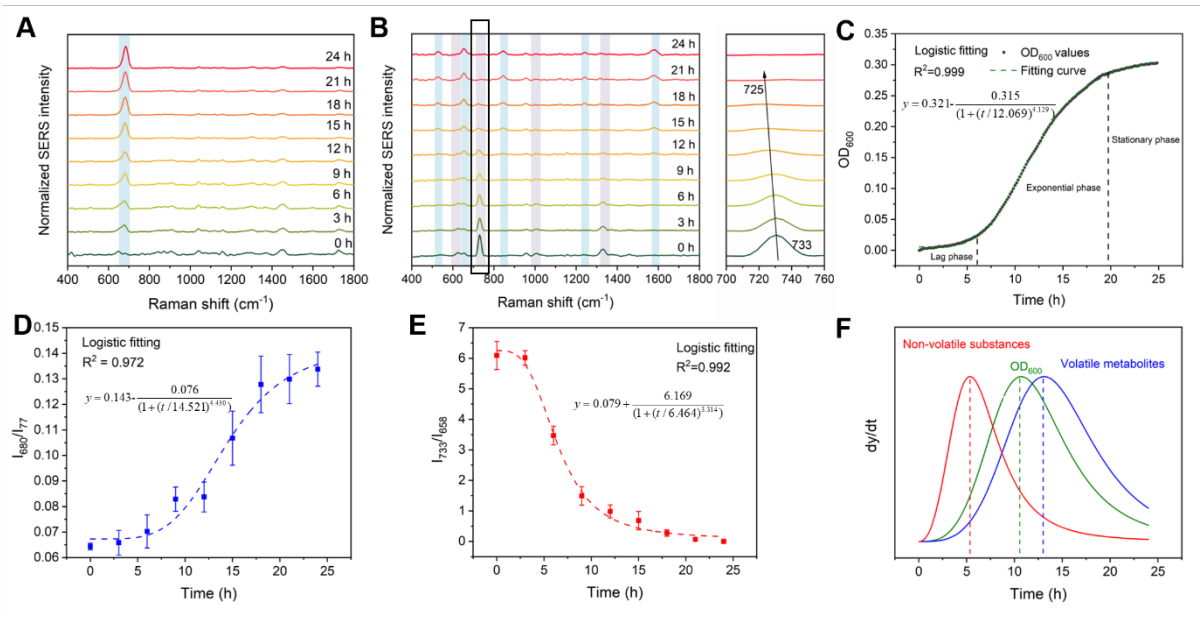

Figure 3. (A) SERS spectra collected for volatile metabolites at 3 h intervals with the intensities normalized by I_{77}; (B) SERS spectra collected for non-volatile substances at 3 h intervals with the intensities normalized by I_{77}, the right panel highlights the shift of peak 733 cm^{-1} to 725 cm^{-1}; The light blue bars indicate the characteristic peaks of bacterial metabolites while the light red bars refer to the LB medium peaks that decrease; (C) bacterial OD_{600} measured at 10 min intervals and fitted with logistic growth model; (D) kinetics data of I_{680}/I_{77} for volatile metabolites fitted with logistic growth model; (E) kinetics data of I_{733}/I_{658} for non-volatile substances fitted with logistic growth model; (F) signal change rate (dy/dt) of each curve, y reflects I_{680}/I_{77} (DMDS), I_{733}/I_{658} (non-volatile metabolites), or OD_{600} (bacterial growth), respectively.

Bacterial quantification. Following demonstration that the SERS signals of both volatile and non-volatile metabolites can be related to bacterial growth, we next used them to determine the

310 bacterial concentration. We first cultivated different starting concentrations of *P. syringae*
311 within the LB agar plate, measured the OD_{600}, and recorded the SERS signals. As shown in
312 **Figure S8A**, there was an obvious increase in OD_{600} when the concentration was above 10^6
313 CFU/mL following 24 h cultivation. For lower starting concentrations, the OD_{600} signal could
314 not be differentiated from the control. For the DMDS SERS signal, the concentration where
315 there was a significant change in I_{680}/I_{77} was at 10^7 CFU/mL (**Figure S8B**), which was 10×
316 higher than that based on OD_{600}. We infer that the relatively low concentration of DMDS (<5
317 nM) when diluted within the headspace increased the detection limit. Compared to OD_{600} and
318 the DMDS signal, quantification of non-volatile metabolites (I_{733}/I_{658}) was improved over a
319 lower initial concentration range (10^5 to 10^8 CFU/mL). When the concentration of *P. syringae*
320 exceeded 10^8 CFU/mL, I_{733}/I_{658} plateaued. In this case, I_{733}/I_{658} no longer changed due to the
321 complete consumption of nutrients within LB. The combined SERS signals for both DMDS
322 and nonvolatile substances can be used for bacterial quantification with good performance.
323 **Diagnosis of viral infections.** In real-world systems, bacterial metabolism can be affected by
324 environmental conditions, especially following viral infection.[64,65] The resulting alteration of
325 bacterial metabolism may result in changes in the SERS signal. *P. syringae* was exposed to
326 lytic bacteriophage Phi6 for 24 h and SERS spectra were collected. As shown in **Figure 4A**,
327 following incubation with Phi6, no peaks arose for the volatile metabolites of *P. syringae*.
328 Instead, the normalized intensities of the original peaks (e.g., I_{680}/I_{77}) decreased. The higher the
329 initial Phi6 concentration, the greater the decline in the I_{680}/I_{77} ratio. This result suggests that
330 Phi6 infection impedes DMDS production. The relative decrease in the DMDS SERS intensity
331 can be used for Phi6 quantification. **Figure 4B** depicts the plot of I_{680}/I_{77} versus the initial Phi6
332 concentration. When the concentration ranged from 500 PFU to 50,000 PFU, I_{680}/I_{77} exhibited
333 a good linear relationship versus the logarithm of the bacterial concentration.
334 The relationship between the SERS signal and phi6 concentration was more complicated

335 for non-volatile substances. As discussed previously, LB agar had a strong peak at ~733 cm^{-1},
336 which gradually shifted to ~725 cm^{-1} and diminished during *P. syringae* cultivation. After 24
337 h, this peak completely disappeared and the peak at 658 cm^{-1} dominated. In the presence of
338 Phi6, the SERS spectrum reflects an intermediate state between the fresh LB agar plate and 24
339 h incubated *P. syringae* (**Figure 4C**). Both peaks at 725-733 cm^{-1} and 658 cm^{-1} had strong
340 intensities in the presence of Phi6. The peak ratio (I_{733}/I_{658}) changed with the initial Phi6
341 concentration and can be used for quantification. A linear relationship between I_{733}/I_{658} and the
342 logarithm of Phi6 concentration was observed between 1,200 PFU and 50,000 PFU (**Figure**
343 **4D**).

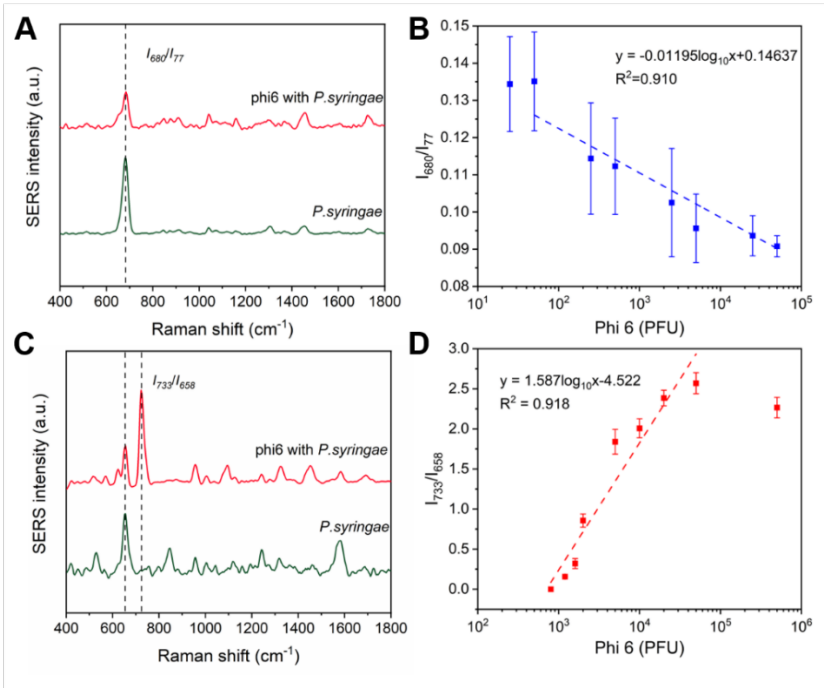

344

345 **Figure 4**. (A) SERS spectra of volatile metabolites of uninfected *P. syringae* and Phi6 (50,000
346 PFU) infected *P. syringae*; (B) the linear relationship between I_{680}/I_{77} and logarithm of Phi6
347 concentration (500-50,000 PFU); (C) SERS spectra of nonvolatile substances of *P. syringae*
348 and Phi6 (10,000 PFU) infected *P. syringae*; (B) the linear relationship between I_{733}/I_{658} and
349 logarithm of Phi6 concentration (1,200-50,000PFU).
350

351 It should be noted that the peak ratio changes detected for the non-volatile substances are
352 do not uniquely reflect Phi6 infection. As discussed previously, both the cultivation time and
353 the concentration of *P. syringae* can alter the ratio. For example, Phi6 (~10^4 PFU) infected *P.*

354 *syringae* (~10^9 CFU/mL) (**Figure 5A, curve a**) and *P. syringae* with a lower concentration
355 (~10^7 CFU/mL) (**Figure 5A, curve b**) had similar I_{733}/I_{658} ratios. It is possible, however, to
356 use the entire SERS spectrum for viral infection diagnosis and unknown sample classification.
357 To illustrate, we identified the 18 peaks present in both the *P. syringae* sample and in the Phi6
358 infected *P. syringae* sample and normalized the spectra using I_{733}. Assignments of these peaks
359 are listed in **Table S3**. Compared with *P. syringae* alone, the Phi6 infected *P. syringae* sample
360 had an increased peak intensity at 957 cm^{-1} (phosphate or C=C deformation), but lower peak
361 intensities at 526 (S-S disulfide stretch in proteins), 842 (glucose), 1092 (C-C skeletal and C-
362 O-C stretching from glycosidic link), and 1582 cm^{-1} (phenylalanine). Previous studies have
363 shown that compared with uninfected controls, extracellular metabolites in phage infected
364 bacterial samples have decreased concentrations.[64] The decrease suggests that surviving cells
365 in the virus-infected cultures consumed materials from the lysed cells to support their
366 metabolism, consequently depleting the selected metabolites and resulting in lower SERS
367 intensities. Such subtle discrepancies cannot be differentiated by visual inspection of the SERS
368 spectra. To achieve improved statistical classification, multivariate analysis was used to
369 analyze the spectroscopic data.[66-68] We used PCA to reduce the dimensionality of the 3600
370 spectra collected from Phi6 infected samples and uninfected controls (2000 spectra for Phi6
371 infected samples and 1600 spectra for uninfected controls). The first nine principal PCs (≈95%
372 of total spectral variance) were used for SVM classification. The classification results are
373 summarized in **Figure 5B** in a confusion matrix form that indicates an overall accuracy of 93%
374 can be achieved using SVM with a quadratic kernel. The sensitivity and specificity were 92.8%
375 and 93.3%, respectively, as calculated from the PCA-SVM confusion matrix (**Table S4**).

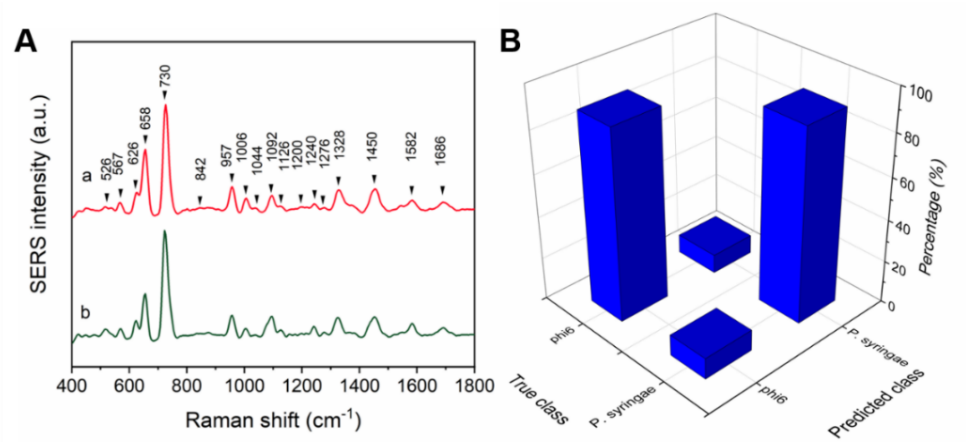

Figure 5. (A) SERS spectra of non-volatile substances of a) 10^4 PFU Phi6 infected 10^9 CFU/mL *P. syringae*; b), 10^7 CFU/mL *P. syringae*; (B) Histograms of confusion matrix for PCA-SVM (n = 2000 for 10^4 PFU Phi6 infected 10^9 CFU/mL *P. syringae* and n = 1600 for 10^7 CFU/mL *P. syringae*).

Environmental Implications. This study demonstrates the application of SERS detection of bacterial metabolites for both monitoring bacterial growth and diagnosis of viral infection. This method integrates the SERS signals of volatile metabolites in the headspace above a culture plate and non-volatile substances in the plate, thus providing detailed information about nutrient consumption, metabolite production, and bacterial growth. Compared with other conventional analytical methods, the present approach is especially promising for environmental analysis. Firstly, it can enable precise and rapid identification of bacteria without labor-intensive pretreatment work. Bacteria are ubiquitous and different sampling techniques as well as pretreatment methods are often required when sampling each matrix (e.g., water, soil, and air). The reported method is based on bacterial culturing and metabolic sensing and therefore, minimal pretreatment was required. The SERS results show comparable quantitative performance to classic culture based optical density measurements. Furthermore, the SERS tape is readily field-deployable, which can overcome sampling difficulties and minimize disturbances caused by the sampling process, especially in confined environments. We applied the same methodology to monitor another bacterium (*E. coli*) and its bacteriophage MS2. As expected, *E. coli* exhibits a different SERS pattern from *P. syringae* (**Figure S9A**).

398 Such spectral variation suggests that the fingerprint SERS profiles of these metabolites can
399 enable accurate identification of bacterial species. When infected by bacteriophages, the host
400 bacterial metabolism was altered in favor of viral replication and the alterations in the SERS
401 signal, when coupled with multivariate analysis, can be used to diagnose viral infections. Our
402 method could be successfully extended to diagnose MS2 infection by monitoring the
403 metabolism of its host bacterium *E. coli* (**Figure S9B**). The results for both Phi6 and MS2
404 suggest that we can potentially apply this approach to measure other virus-cell interactions.
405 Compared with traditional PCR, this method is capable to detect viable viruses and the SERS
406 spectra can be collected on-site with the help of a portable Raman spectrometer. The results
407 not only provide an alternative viral sensing method, but also suggest a feasible pathway to
408 examine how environmental stimuli (pH, salinity, temperature, nutrients, antibiotics etc.) affect
409 bacterial growth.
410

411 **ASSOCIATED CONTENT**

412 Additional information of SERS substrate characterization, Optical images with SERS results
413 of *P. syringae* in a scan area, SERS results for DMDS quantification, PCA results, SVM results,
414 SERS intensities of featured peaks, bacterial quantification results, SERS results for *E. coli* and
415 MS2, bacterial metabolite list, kinetics fitting results, and SERS peak assignments (Figures S1-
416 S9 and Tables S1-S4).
417

418 **ACKNOWLEDGEMENT**

419 This research was supported by the US National Science Foundation grants OISE-1545756 and
420 CBET-2029911. Laboratory and instrumentation support was provided by NanoEarth – a node
421 of the NSF supported NNCI (NSF award number #1542100). Additional support was provided
422 by the Sustainable Nanotechnology Interdisciplinary Graduate Program (VTSuN IGEP)

funded by the Virginia Tech Graduate School.

REFERENCES

(1) Audrain, B.; Farag, M. A.; Ryu, C.-M.; Ghigo, J.-M., Role of bacterial volatile compounds in bacterial biology. *FEMS Microbiol. Rev.* **2015,** *39*, 222-233.

(2) Findlay, B. L., The chemical ecology of predatory soil bacteria. *ACS Chem. Biol.* **2016,** *11*, 1502-1510.

(3) Modolon, F.; Barno, A. R.; Villela, H. D.; Peixoto, R. S., Ecological and biotechnological importance of secondary metabolites produced by coral-associated bacteria. *J. Appl. Microbiol.* **2020,** *129*, 1441-1457.

(4) Tyc, O.; Song, C.; Dickschat, J. S.; Vos, M.; Garbeva, P., The ecological role of volatile and soluble secondary metabolites produced by soil bacteria. *Trends Microbiol.* **2017,** *25*, 280-292.

(5) Tannous, J.; Atoui, A.; El Khoury, A.; Francis, Z.; Oswald, I. P.; Puel, O.; Lteif, R., A study on the physicochemical parameters for *Penicillium expansum* growth and patulin production: effect of temperature, pH, and water activity. *Food Sci. Nutr.* **2016,** *4*, 611-622.

(6) Covington, B. C.; Spraggins, J. M.; Ynigez-Gutierrez, A. E.; Hylton, Z. B.; Bachmann, B. O., Response of secondary metabolism of hypogean actinobacterial genera to chemical and biological stimuli. *Appl. Environ. Microbiol.* **2018,** *84*, e01125-18.

(7) Dickschat, J. S., Quorum sensing and bacterial biofilms. *Nat. Prod. Rep.* **2010,** *27*, 343-369.

(8) Šmajs, D.; Micenková, L.; Šmarda, J.; Vrba, M.; Ševčíková, A.; Vališová, Z.; Woznicová, V., Bacteriocin synthesis in uropathogenic and commensal *Escherichia coli*: colicin E1 is a potential virulence factor. *BMC Microbiol.* **2010,** *10*, 1-10.

(9) Lewis, J. M.; Savage, R. S.; Beeching, N. J.; Beadsworth, M. B.; Feasey, N.; Covington, J. A., Identifying volatile metabolite signatures for the diagnosis of bacterial respiratory tract infection using electronic nose technology: a pilot study. *PLoS One* **2017,** *12*, e0188879.

(10) Walton, C.; Fowler, D. P.; Turner, C.; Jia, W.; Whitehead, R. N.; Griffiths, L.; Dawson, C.; Waring, R. H.; Ramsden, D. B.; Cole, J. A., Analysis of volatile organic compounds of bacterial origin in chronic gastrointestinal diseases. *Inflamm. Bowel Dis.* **2013,** *19*, 2069-2078.

(11) Heaney, L. M., Applying mass spectrometry-based assays to explore gut microbial metabolism and associations with disease. *Clin. Chem. Lab. Med.* **2020,** *58*, 719-732.

(12) Tait, E.; Perry, J. D.; Stanforth, S. P.; Dean, J. R., Identification of volatile organic compounds produced by bacteria using HS-SPME-GC-MS. *J. Chromatogr. Sci.* **2014,** *52*, 363-373.

(13) Vishwanath, V.; Sulyok, M.; Labuda, R.; Bicker, W.; Krska, R., Simultaneous determination of 186 fungal and bacterial metabolites in indoor matrices by liquid chromatography/tandem mass spectrometry. *Anal. Bioanal. Chem.* **2009,** *395*, 1355-1372.

(14) Lawal, O.; Knobel, H.; Weda, H.; Nijsen, T. M.; Goodacre, R.; Fowler, S. J., TD/GC-MS analysis of volatile markers emitted from mono-and co-cultures of *Enterobacter cloacae* and *Pseudomonas aeruginosa* in artificial sputum. *Metabolomics* **2018,** *14*, 66.

(15) Sismaet, H. J.; Pinto, A. J.; Goluch, E. D., Electrochemical sensors for identifying pyocyanin production in clinical *Pseudomonas aeruginosa* isolates. *Biosens. Bioelectron.* **2017,** *97*, 65-69.

(16) Wilson, A. D., Application of electronic-nose technologies and VOC-biomarkers for the noninvasive early diagnosis of gastrointestinal diseases. *Sensors* **2018,** *18*, 2613.

(17) Simoska, O.; Sans, M.; Fitzpatrick, M. D.; Crittenden, C. M.; Eberlin, L. S.; Shear, J. B.; Stevenson, K. J., Real-time electrochemical detection of *Pseudomonas aeruginosa* phenazine metabolites using transparent carbon ultramicroelectrode arrays. *ACS Sens.* **2018,** *4*, 170-179.

(18) Molina, B. G.; del Valle, L. J.; Turon, P.; Armelin, E.; Alemán, C., Electrochemical sensor for bacterial metabolism based on the detection of NADH by Polythiophene nanoparticles. *J. Phys. Chem. C* **2019,** *123*, 22181-22190.

(19) Hong, S.; Zheng, D.-W.; Zhang, Q.-L.; Deng, W.-W.; Song, W.-F.; Cheng, S.-X.; Sun, Z.-J.; Zhang, X.-Z., An RGB-emitting molecular cocktail for the detection of bacterial fingerprints. *Chem. Sci.* **2020,** *11*, 4403-4409.

(20) Zong, C.; Xu, M.; Xu, L.-J.; Wei, T.; Ma, X.; Zheng, X.-S.; Hu, R.; Ren, B., Surface-enhanced Raman spectroscopy for bioanalysis: reliability and challenges. *Chem. Rev.* **2018,** *118*, 4946-4980.

(21) Cialla-May, D.; Zheng, X.-S.; Weber, K.; Popp, J., Recent progress in surface-enhanced Raman spectroscopy for biological and biomedical applications: from cells to clinics. *Chem. Soc. Rev.* **2017,** *46*, 3945-3961.

(22) Schlücker, S., Surface-Enhanced raman spectroscopy: Concepts and chemical applications. *Angew. Chem. Int. Ed.* **2014,** *53*, 4756-4795.

(23) Kao, Y.-C.; Han, X.; Lee, Y. H.; Lee, H. K.; Phan-Quang, G. C.; Lay, C. L.; Sim, H. Y. F.; Phua, V. J. X.; Ng, L. S.; Ku, C. W., Multiplex surface-enhanced Raman scattering

488 identification and quantification of urine metabolites in patient samples within 30 min. *ACS*
489 *Nano* **2020,** *14*, 2542-2552.
490 (24) Tait, E.; Stanforth, S. P.; Reed, S.; Perry, J. D.; Dean, J. R., Analysis of pathogenic
491 bacteria using exogenous volatile organic compound metabolites and optical sensor detection.
492 *RSC adv.* **2015,** *5*, 15494-15499.
493 (25) Morelli, L.; Centorbi, F. A.; Ilchenko, O.; Jendresen, C. B.; Demarchi, D.; Nielsen, A. T.;
494 Zór, K.; Boisen, A., Simultaneous quantification of multiple bacterial metabolites using
495 surface-enhanced Raman scattering. *Analyst* **2019,** *144*, 1600-1607.
496 (26) Liu, J.; Cai, C.; Wang, Y.; Liu, Y.; Huang, L.; Tian, T.; Yao, Y.; Wei, J.; Chen, R.; Zhang,
497 K., A biomimetic plasmonic nanoreactor for reliable metabolite detection. *Adv. Sci.* **2020,** *7*,
498 1903730.
499 (27) Bodelón, G.; Montes-García, V.; López-Puente, V.; Hill, E. H.; Hamon, C.; Sanz-Ortiz,
500 M. N.; Rodal-Cedeira, S.; Costas, C.; Celiksoy, S.; Pérez-Juste, I., Detection and imaging of
501 quorum sensing in *Pseudomonas aeruginosa* biofilm communities by surface-enhanced
502 resonance Raman scattering. *Nat. Mater.* **2016,** *15*, 1203-1211.
503 (28) DeJong, C. S.; Wang, D. I.; Polyakov, A.; Rogacs, A.; Simske, S. J.; Shkolnikov, V.,
504 Bacterial detection and differentiation via direct volatile organic compound sensing with
505 surface enhanced Raman spectroscopy. *Chemistryselect* **2017,** *2*, 8431-8435.
506 (29) Guo, J.; Liu, Y.; Yang, Y.; Li, Y.; Wang, R.; Ju, H., A filter supported surface-enhanced
507 Raman scattering "nose" for point-of-care monitoring of gaseous metabolites of bacteria. *Anal.*
508 *Chem.* **2020,** *92*, 5055-5063.
509 (30) Kelly, J.; Patrick, R.; Patrick, S.; Bell, S. E., Surface-enhanced Raman spectroscopy for
510 the detection of a metabolic product in the headspace above live bacterial cultures. *Angew.*
511 *Chem. Int. Ed.* **2018,** *57*, 15686-15690.
512 (31) Nguyen, C. Q.; Thrift, W. J.; Bhattacharjee, A.; Ranjbar, S.; Gallagher, T.; Darvishzadeh-
513 Varcheie, M.; Sanderson, R. N.; Capolino, F.; Whiteson, K.; Baldi, P., Longitudinal monitoring
514 of biofilm formation via robust surface-enhanced Raman scattering quantification of
515 *Pseudomonas aeruginosa*-produced metabolites. *ACS Appl. Mater. Interfaces* **2018,** *10*, 12364-
516 12373.
517 (32) Bodelón, G.; Montes-García, V.; Costas, C.; Pérez-Juste, I.; Pérez-Juste, J.; Pastoriza-
518 Santos, I.; Liz-Marzán, L. M., Imaging bacterial interspecies chemical interactions by surface-
519 enhanced Raman scattering. *ACS Nano* **2017,** *11*, 4631-4640.
520 (33) De Marchi, S.; Bodelon, G.; Vazquez-Iglesias, L.; Liz-Marzan, L. M.; Perez-Juste, J.;

521 Pastoriza-Santos, I., Surface-enhanced Raman scattering (SERS) imaging of bioactive
522 metabolites in mixed bacterial populations. *Appl. Mater. Today* **2019,** *14*, 207-215.
523 (34) Guo, J.; Liu, Y.; Chen, Y.; Li, J.; Ju, H., A multifunctional SERS sticky note for real-time
524 quorum sensing tracing and inactivation of bacterial biofilms. *Chem. Sci.* **2018,** *9*, 5906-5911.
525 (35) Wang, P.; Wang, X.; Sun, Y.; Gong, G.; Fan, M.; He, L., Rapid identification and
526 quantification of the antibiotic susceptibility of lactic acid bacteria using surface enhanced
527 Raman spectroscopy. *Anal. Methods* **2020,** *12*, 376-382.
528 (36) Chang, K.-W.; Cheng, H.-W.; Shiue, J.; Wang, J.-K.; Wang, Y.-L.; Huang, N.-T.,
529 Antibiotic susceptibility test with surface-enhanced Raman scattering in a microfluidic system.
530 *Anal. Chem.* **2019,** *91*, 10988-10995.
531 (37) Breitbart, M.; Bonnain, C.; Malki, K.; Sawaya, N. A., Phage puppet masters of the marine
532 microbial realm. *Nat. Microbiol.* **2018,** *3*, 754-766.
533 (38) Snyder, A. B.; Perry, J. J.; Yousef, A. E., Developing and optimizing bacteriophage
534 treatment to control enterohemorrhagic *Escherichia coli* on fresh produce. *Int. J. Food*
535 *Microbiol.* **2016,** *236*, 90-97.
536 (39) Kakasis, A.; Panitsa, G., Bacteriophage therapy as an alternative treatment for human
537 infections. A comprehensive review. *Int. J. Antimicrob. Agents* **2019,** *53*, 16-21.
538 (40) Lin, K.; Marr, L. C., Humidity-dependent decay of viruses, but not bacteria, in aerosols
539 and droplets follows disinfection kinetics. *Environ. Sci. Technol.* **2019,** *54*, 1024-1032.
540 (41) Aquino de Carvalho, N.; Stachler, E. N.; Cimabue, N.; Bibby, K., Evaluation of Phi6
541 persistence and suitability as an enveloped virus surrogate. *Environ. Sci. Technol.* **2017,** *51*,
542 8692-8700.
543 (42) Fedorenko, A.; Grinberg, M.; Orevi, T.; Kashtan, N., Survival of the enveloped
544 bacteriophage Phi6 (a surrogate for SARS-CoV-2) in evaporated saliva microdroplets
545 deposited on glass surfaces. *Sci. Rep.* **2020,** *10*, 22419.
546 (43) Lin, K.; Marr, L. C., Aerosolization of Ebola virus surrogates in wastewater systems.
547 *Environ. Sci. Technol.* **2017,** *51*, 2669-2675.
548 (44) Leopold, N.; Lendl, B., A new method for fast preparation of highly surface-enhanced
549 Raman scattering (SERS) active silver colloids at room temperature by reduction of silver
550 nitrate with hydroxylamine hydrochloride. *J. Phys. Chem. B* **2003,** *107*, 5723-5727.
551 (45) Chen, J.; Huang, Y.; Kannan, P.; Zhang, L.; Lin, Z.; Zhang, J.; Chen, T.; Guo, L., Flexible
552 and adhesive surface enhance Raman scattering active tape for rapid detection of pesticide
553 residues in fruits and vegetables. *Anal. Chem.* **2016,** *88*, 2149-2155.

(46) Stranahan, S. M.; Willets, K. A., Super-resolution optical imaging of single-molecule SERS hot spots. *Nano Lett.* **2010,** *10*, 3777-3784.

(47) Zhou, H.; Yang, D.; Ivleva, N. P.; Mircescu, N. E.; Niessner, R.; Haisch, C., SERS detection of bacteria in water by in situ coating with Ag nanoparticles. *Anal. Chem.* **2014,** *86*, 1525-1533.

(48) Wei, H.; Leng, W.; Song, J.; Liu, C.; Willner, M. R.; Huang, Q.; Zhou, W.; Vikesland, P. J., Real-time monitoring of ligand exchange kinetics on gold nanoparticle surfaces enabled by hot spot-normalized surface-enhanced Raman scattering. *Environ. Sci. Technol.* **2018,** *53*, 575-585.

(49) Wei, H.; Leng, W.; Song, J.; Willner, M. R.; Marr, L. C.; Zhou, W.; Vikesland, P. J., Improved quantitative SERS enabled by surface plasmon enhanced elastic light scattering. *Anal. Chem.* **2018,** *90*, 3227-3237.

(50) Wei, H.; McCarthy, A.; Song, J.; Zhou, W.; Vikesland, P. J., Quantitative SERS by hot spot normalization–surface enhanced Rayleigh band intensity as an alternative evaluation parameter for SERS substrate performance. *Faraday Discuss.* **2017,** *205*, 491-504.

(51) Viehrig, M.; Thilsted, A. H.; Matteucci, M.; Wu, K.; Catak, D.; Schmidt, M. S.; Zór, K.; Boisen, A., Injection-molded microfluidic device for SERS sensing using embedded Au-capped polymer nanocones. *ACS Appl. Mater. Interfaces* **2018,** *10*, 37417-37425.

(52) Polavarapu, L.; Porta, A. L.; Novikov, S. M.; Coronado-Puchau, M.; Liz-Marzán, L. M., Pen-on-paper approach toward the design of universal surface enhanced Raman scattering substrates. *Small* **2014,** *10*, 3065-3071.

(53) Effmert, U.; Kalderás, J.; Warnke, R.; Piechulla, B., Volatile mediated interactions between bacteria and fungi in the soil. *J. Chem. Ecol.* **2012,** *38*, 665-703.

(54) Meldau, D. G.; Meldau, S.; Hoang, L. H.; Underberg, S.; Wünsche, H.; Baldwin, I. T., Dimethyl disulfide produced by the naturally associated bacterium *Bacillus* sp B55 promotes *Nicotiana attenuata* growth by enhancing sulfur nutrition. *Plant Cell* **2013,** *25*, 2731-2747.

(55) Movasaghi, Z.; Rehman, S.; Rehman, I. U., Raman spectroscopy of biological tissues. *Appl. Spectrosc. Rev.* **2007,** *42*, 493-541.

(56) Cellini, A.; Biondi, E.; Buriani, G.; Farneti, B.; Rodriguez-Estrada, M. T.; Braschi, I.; Savioli, S.; Blasioli, S.; Rocchi, L.; Biasioli, F., Characterization of volatile organic compounds emitted by kiwifruit plants infected with *Pseudomonas syringae* pv. actinidiae and their effects on host defences. *Trees* **2016,** *30*, 795-806.

(57) Li, B.; Sirimuthu, N. M.; Ray, B. H.; Ryder, A. G., Using surface-enhanced Raman

587 scattering (SERS) and fluorescence spectroscopy for screening yeast extracts, a complex
588 component of cell culture media. *J. Raman Spectrosc.* **2012,** *43*, 1074-1082.
589 (58) Marotta, N. E.; Bottomley, L. A., Surface-enhanced Raman scattering of bacterial cell
590 culture growth media. *Appl. Spectrosc.* **2010,** *64*, 601-606.
591 (59) Witkowska, E.; Niciński, K.; Korsak, D.; Szymborski, T.; Kamińska, A., Sources of
592 variability in SERS spectra of bacteria: comprehensive analysis of interactions between
593 selected bacteria and plasmonic nanostructures. *Anal. Bioanal. Chem.* **2019,** *411*, 2001-2017.
594 (60) Hafez, R. M.; Abdel-Rahman, T. M.; Naguib, R. M., Uric acid in plants and
595 microorganisms: Biological applications and genetics-A review. *J. Adv. Res.* **2017,** *8*, 475-486.
596 (61) Xi, H.; Schneider, B. L.; Reitzer, L., Purine catabolism in *Escherichia coli* and function
597 of xanthine dehydrogenase in purine salvage. *J. Bacteriol.* **2000,** *182*, 5332-5341.
598 (62) El-Zahry, M. R.; Mahmoud, A.; Refaat, I. H.; Mohamed, H. A.; Bohlmann, H.; Lendl, B.,
599 Antibacterial effect of various shapes of silver nanoparticles monitored by SERS. *Talanta* **2015,**
600 *138*, 183-189.
601 (63) Pinheiro, L. A.; Pereira, C.; Barreal, M. E.; Gallego, P. P.; Balcão, V. M.; Almeida, A.,
602 Use of phage ϕ6 to inactivate *Pseudomonas syringae* pv. *actinidiae* in kiwifruit plants: In vitro
603 and ex vivo experiments. *Appl. Microbiol. Biotechnol.* **2020,** *104*, 1319-1330.
604 (64) Ankrah, N. Y. D.; May, A. L.; Middleton, J. L.; Jones, D. R.; Hadden, M. K.; Gooding,
605 J. R.; LeCleir, G. R.; Wilhelm, S. W.; Campagna, S. R.; Buchan, A., Phage infection of an
606 environmentally relevant marine bacterium alters host metabolism and lysate composition.
607 *ISME J.* **2014,** *8*, 1089-1100.
608 (65) Zimmerman, A. E.; Howard-Varona, C.; Needham, D. M.; John, S. G.; Worden, A. Z.;
609 Sullivan, M. B.; Waldbauer, J. R.; Coleman, M. L., Metabolic and biogeochemical
610 consequences of viral infection in aquatic ecosystems. *Nat. Rev. Microbiol.* **2019**, 1-14.
611 (66) Kim, W.; Lee, S. H.; Kim, J. H.; Ahn, Y. J.; Kim, Y.-H.; Yu, J. S.; Choi, S., Paper-based
612 surface-enhanced Raman spectroscopy for diagnosing prenatal diseases in women. *ACS Nano*
613 **2018,** *12*, 7100-7108.
614 (67) Nam, W.; Ren, X.; Tali, S. A. S.; Ghassemi, P.; Kim, I.; Agah, M.; Zhou, W., Refractive-
615 index-insensitive nanolaminated SERS substrates for label-free raman profiling and
616 classification of living cancer cells. *Nano Lett.* **2019,** *19*, 7273-7281.
617 (68) Lussier, F. l.; Missirlis, D.; Spatz, J. P.; Masson, J.-F., Machine-learning-driven surface-
618 enhanced Raman scattering optophysiology reveals multiplexed metabolite gradients near cells.
619 *ACS Nano* **2019,** *13*, 1403-1411.

620